Atmos. Chem. Phys. Discuss., 9, 6855–6887, 2009
www.atmos-chem-phys-discuss.net/9/6855/2009/

Atmospheric Chemistry and Physics Discussions

This discussion paper is/has been under review for the journal *Atmospheric Chemistry and Physics (ACP)*. Please refer to the corresponding final paper in *ACP* if available.

A new insight on tropospheric methane in the Tropics – first year from IASI hyperspectral infrared observations

C. Crevoisier[1], D. Nobileau[1], A. M. Fiore[2], R. Armante[1], A. Chédin[1], and N. A. Scott[1]

[1]Laboratoire de Météorologie Dynamique/CNRS/IPSL, Ecole Polytechnique, Palaiseau, France
[2]Geophysical Fluid Dynamics Laboratory/NOAA, Princeton, New Jersey, USA

Received: 21 January 2009 – Accepted: 9 February 2009 – Published: 12 March 2009

Correspondence to: C. Crevoisier (cyril.crevoisier@lmd.polytechnique.fr)

Published by Copernicus Publications on behalf of the European Geosciences Union.

Abstract

Simultaneous observations from the Infrared Atmospheric Sounding Interferometer (IASI) and from the Advanced Microwave Sounding Unit (AMSU), launched together onboard the European MetOp platform in October 2006, are used to retrieve a mid-to-upper tropospheric content of methane (CH_4) in clear-sky conditions, in the Tropics, over sea, for the first 16 months of operation of MetOp (July 2007–October 2008). With its very high spectral resolution, IASI provides nine channels in the 7.7 μm band highly sensitive to CH_4 with reduced sensitivities to other atmospheric variables. These channels, sensitive to both CH_4 and temperature, are used in conjunction with AMSU channels, only sensitive to temperature, to decorrelate both signals through a non-linear inference scheme based on neural networks. A key point of this approach is that no use is made of prior information in terms of methane seasonality, trend, or geographical patterns. The accuracy of the retrieval is estimated to be about 16 ppbv (~0.9%). Features of the retrieved methane space-time distribution include: (1) a strong seasonal cycle of 30 ppbv in the Northern Tropics with a maximum in January–March and a minimum in July–September, and a flat seasonal cycle in the Southern Tropics, in agreement with in-situ measurements; (2) a latitudinal decrease of 30 ppbv from 20° N to 20° S, in boreal spring and summer, lower than what is observed at the surface but in excellent agreement with tropospheric aircraft measurements; (3) geographical patterns in good agreement with simulations from the atmospheric transport and chemistry model MOZART-2, but with a higher variability and a higher concentration in boreal winter; (4) signatures of CH_4 emissions transported to the middle troposphere such as a large plume of elevated tropospheric methane south of the Asian continent, which might be due to Asian emissions from rice paddies uplifted by deep convection during the monsoon period and then transported towards Indonesia. In addition to bringing a greatly improved view of methane distribution, these results from IASI should provide a means to observe and understand atmospheric transport pathways of methane from the surface to the upper troposphere.

1 Introduction

Knowledge of today's methane (CH_4) sources and sinks, their spatial distribution and their variability in time is essential for predicting the future CH_4 atmospheric concentration levels, which is second only to carbon dioxide (CO_2) as an important human-caused greenhouse gas (IPCC, 2007). In particular, the Tropics are crucial to global budgets of methane. Tropical wetlands are believed to be a considerable CH_4 source (e.g., Cicerone et al., 1988; Prentice et al., 2001; Mikaloff-Fletcher et al., 2004a; Chen et al., 2006; Bousquet et al., 2006), as well as emissions from rice paddies (Huang et al., 2004) and termites. Tropical deforestation is also associated with considerable emissions of CH_4, since the bulk of this deforestation is accomplished through fires. The Tropics also play a major role in CH_4 and carbon monoxide (CO) chemistry, due to the considerable photochemical production of OH in these regions (e.g., Spivakovsky et al., 2000), which is the main sink of methane by globally removing about 85% of methane molecules emitted to the atmosphere (e.g., Logan et al., 1981). However, the exact location, intensity and nature of methane sources and sinks are not as well understood as those for CO_2.

Atmospheric inversions have been widely used to estimate regional fluxes of CH_4 (Houweling et al., 1999; Mikaloff-Fletcher et al., 2004b; Chen et al., 2006; Bousquet et al., 2006). In these approaches, regional fluxes of a given gas to the atmosphere are estimated through the comparison of atmospheric gas concentration observations with atmospheric transport model simulations that describe how surface fluxes influence gas concentrations. Atmospheric inversions have historically relied primarily on in-situ surface observations. This technique generally has the greatest uncertainties in the Tropics, because there are very few in situ observations that effectively constrain these regions (e.g., Rayner and O'Brien, 2001). Furthermore, vigorous tropical convection rapidly transports methane to high altitudes, so that these fluxes are not easily detected by surface observations. By densely sampling the atmosphere in time and space, satellite measurements of the distribution of global atmospheric CH_4 concen-

tration would in principle fill this gap in scale.

In recent years, several instruments have given access to information on the distribution of methane in various parts of the atmosphere. Measurements made by the Halogen Occultation Experiment (HALOE) on the Upper Atmosphere Research Satellite (UARS) (Schoeberl et al., 1995; Park et al., 1996; Randel et al., 1998) have provided information on methane in the stratosphere. Tropospheric columns of methane have been retrieved from observations made in the infrared by the Interferometric Monitor for Greenhouse Gases (IMG) flying on board the Japanese Advanced Earth Observing Satellite (ADEOS) (Clerbaux et al., 2003), but because of satellite failure, only a few months of observation are available. Total columns of methane have also been retrieved, mostly over land, from near infrared observations by the Scanning Imaging Absorption spectroMeter for Atmospheric CHartographY (SCIAMACHY) instrument on board the European Space Agency's environmental research satellite (ENVISAT) (Frankenberg et al., 2005, 2006, 2008; Buchwitz et al., 2006). More recently, global CH_4 distribution, mostly representative of the middle to upper troposphere, have been retrieved using observations from the Atmospheric Infrared Sounder (AIRS) on the EOS/Aqua platform (Xiong et al., 2008).

With its 8461 channels covering most of the infrared spectrum at a very high spectral resolution, the Infrared Atmospheric Sounding Interferometer (IASI) launched onboard the European MetOp platform in October 2006, gives the opportunity to use several channels specifically sensitive to CH_4, and to improve our presently quite limited knowledge of its tropospheric distribution. CH_4 infrared measurements being sensitive to both temperature and CH_4 variations, an independent information on temperature is needed to allow separating these two effects. Also flying onboard MetOp, the Advanced Microwave Sounding Unit (AMSU) provides microwave observations only sensitive to temperature that can be used to reach this goal. This study is focused on the tropical belt (20° N, 20° S) where higher-quality retrievals are expected compared to the extratropics because of the low variability of the temperature profiles.

The goals of this paper are to present the first sixteen months of methane retrieved

from MetOp IASI/AMSU observations. Section 2 describes data and modeling tools used in the retrieval process. Section 3 presents the selection of IASI channels based on their sensitivity to methane and other atmospheric variables, along with the non-linear inference scheme used to retrieve a tropospheric integrated content of CH_4. Section 4 describes the retrievals in terms of seasonal cycle, latitudinal variations and geographical distribution, which are analyzed using in-situ data (surface and airborne measurements) and simulations from an atmospheric chemistry and transport model. Section 5 gives the conclusion.

2 Data and modeling tools

2.1 Satellite data: IASI and AMSU

The Infrared Atmospheric Sounding Interferometer (IASI) developed by the Centre National d'Etudes Spatiales (CNES) in collaboration with the European Organisation for the Exploitation of Meteorological Satellites (EUMETSAT) is a Fourier Transform Spectrometer based on a Michelson Interferometer coupled to an integrated imaging system that measures infrared radiation emitted from the Earth. IASI provides 8461 spectral samples, aligned in three bands between 645.00 cm^{-1} and 2760.00 cm^{-1} (15.5 μm and 3.63 μm), with a spectral resolution of 0.50 cm^{-1} after apodisation ("Level 1c" spectra). The spectral sampling interval is 0.25 cm^{-1}. IASI is an across track scanning system with scan range of ±48.3°, symmetrically with respect to the nadir direction. A nominal scan line covers 30 scan positions towards the Earth. The instantaneous field of view (IFOV) has a ground resolution of 12 km at nadir.

Also flying onboard MetOp, the Advanced Microwave Sounding Unit (AMSU) is a cross-track scanning total-power radiometer with 15 channels that measure scene radiance in the microwave spectrum from 23.8 to 89.0 GHz. The AMSU instrument has an IFOV of 48 km at nadir, with scan range of ±48.3° from nadir with a total of 30 Earth fields-of-view per scan line. The swath width is approximately 2000 km.

IASI Level 1c and AMSU Level 1b data are available since July 2007. IASI Level 2 data, produced at EUMETSAT, are available for temperature and water vapor since October 2007. Temperature and humidity profiles are given on a 90 level grid. Their estimated accuracies are respectively 1 K and 10% (EUMETSAT, 2004). Both Level 1c and Level 2 data are routinely archived at the Laboratoire de Météorologie Dynamique (LMD) via the Centre for Atmospheric Chemistry Products and Services "Ether" website (http://ether.ipsl.jussieu.fr/), through EUMETCast, the Broadcast System for Environmental Data of EUMETSAT.

2.2 Radiative models and data: 4A and TIGR

Infrared radiative simulations used in this study are performed using the fast line-by-line 4A (Automatized Atmospheric Absorption Atlas) model (Scott and Chédin, 1981) (http://ara.lmd.polytechnique.fr/; http://www.noveltis.fr/4AOP/). Co-developed by LMD and NOVELTIS with the support of CNES, 4A is the reference radiative transfer model for the CNES/EUMETSAT IASI Level 1 Cal/Val and operational processing. Here, it uses spectroscopy from the regularly updated GEISA (Gestion et Etude des Informations Spectroscopiques Atmosphériques: Management and Study of Spectroscopic Information) spectral line data catalog (Jacquinet-Husson et al., 2008).

Our study is based on a statistically representative description of the atmosphere from the Thermodynamic Initial Guess Retrieval (TIGR) database (Chédin et al., 1985; Chevallier et al., 1998), with associated radiative information. Use is made of the latest version of TIGR which comprises 7490 tropical atmospheric situations (4425 over sea, the remaining over land), each of them described by its profiles of temperature, water vapour and ozone. CO_2, CH_4, CO and N_2O reference concentrations are assumed constant along the vertical at 372 ppmv, 1860 ppbv, 100 ppbv and 324 ppbv, respectively. For all TIGR atmospheric situations, for all scan angles, and for the 8461 IASI channels (about 10^9 cases all together), clear-sky brightness temperatures (*BT*), transmittances and Jacobians (partial derivative of the channel *BT* with respect to a layer physical variable such as a gas mixing ratio, a temperature or the emissivity) are com-

puted using 4A. The 15 AMSU BT are computed using the in house STRANSAC microwave forward model.

The noise due to the instrument is also computed using the following equation

$$NE\Delta T\left(T_B(\nu)\right) = NE\Delta T\left(T_{\mathrm{ref}}(\nu)\right)\frac{\frac{\partial B}{\partial T}\left(\nu, T_{\mathrm{ref}}\right)}{\frac{\partial B}{\partial T}\left(\nu, T_B(\nu)\right)} \quad (1)$$

where $NE\Delta T$ is the equivalent noise temperature taken at the brightness temperature T_B, of the channel located at frequency ν, and B is the radiance. The reference noise corresponding to a reference temperature T_{ref} of 280 K is taken from the in-flight noise measurement (CNES, private communication, 2007).

2.3 Atmospheric chemical and transport simulations: MOZART-2

For analyzing the IASI retrievals, use is made of CH_4 mixing ratio fields simulated by the atmospheric chemistry and transport model MOZART-2 (Horowitz et al., 2003), driven by National Center for Environmental Prediction (NCEP) reanalysis with a $1.9^\circ \times 1.9^\circ$ spatial resolution and 29 levels in the vertical. For all species except CH_4, EDGAR v2.0 emissions are used as surface boundary conditions (Horowitz et al., 2003). CH_4 anthropogenic emissions are interpolated using EDGAR 3.2 anthropogenic emission estimates for 1990 and 1995 (Olivier and Berdowski, 2001), and "FAST-TRACK" for 2000 (Olivier et al., 2005). As described in Fiore et al. (2006) (their "ANTHRO+BIO" simulation), emissions for intermediate years are obtained by linear interpolation, with emissions for 2001–2004 held at 2000 values. Wetland CH_4 emissions are from Wang et al. (2004), based on the spatial and seasonal distributions of Matthews and Fung (1987).

3 Methane retrieval method

3.1 Channel selection: Sensitivity study of IASI channels

IASI presents 8461 channels covering most of the infrared spectrum. Only a hundred of them are sensitive to methane. They are either located in band ν_4 of methane, around 7.7 μm (1306 cm^{-1}), or in band ν_3, around 3.8 μm (2630 cm^{-1}), and present various sensitivities to methane and other atmospheric or surface components. The first problem arising in the retrieval method is thus the selection of a set of channels presenting the best properties regarding the retrieval of methane. As described in Crevoisier et al. (2003), three criteria must be used to reach this goal: (1) the sensitivity of the channels to atmospheric CH_4 changes; (2) the sensitivity of the channels to other gases or thermodynamic variables of the atmosphere; (3) the part of the atmosphere to which the channels are sensitive to CH_4 variations.

The sensitivity to methane variations of channels located in the 3.8 μm band is much lower than that of channels located in the 7.7 μm band due to weaker absorption lines: they will not be considered here. In the 7.7 μm band, channels are sensitive to water vapor (H_2O), nitrous oxide (N_2O) and surface characteristics. The corresponding variations, averaged over the TIGR tropical atmospheric situations, are plotted in Fig. 1 in terms of variation of the measured brightness temperature for a variation of 1 K for atmospheric temperature, 10% for CH_4, 20% for H_2O, 2% for N_2O and 0.01 for surface emissivity. The instrument noise is also plotted in Fig. 1.

The main interference, as far as CH_4 is concerned, comes from H_2O, which dominates the infrared spectrum in the methane absorption bands. Since water vapor variability is quite high, especially in the Tropics, and knowledge of its tropospheric distribution still limited, separating the CH_4 signal from water vapor is quite challenging and precludes using most of the channels. Only a few successive channels located in the 1301–1305 cm^{-1} interval (shown with an arrow in Fig. 1) present a low-enough sensitivity to water vapor to be used to retrieve methane. The nine selected channels are given in Table 1, along with their sensitivities and altitude of the maximum of their

associated CH_4 Jacobians. They are not sensitive to nitrous oxide or surface characteristics. For the sake of comparison, only 4 similar AIRS channels, two of them with a slight sensitivity to surface characteristics, are available in the same region (Crevoisier et al., 2003).

Methane Jacobians of the 9 channels are plotted in Fig. 2a. Corresponding temperature and H_2O Jacobians are shown in Fig. 2b and c, respectively. Infrared channels are not sensitive to variations of methane in two parts of the atmosphere: the lower troposphere (roughly below 500 hPa) and the tropopause (Crevoisier et al., 2003). Indeed, for the lower troposphere, an increase of CH_4 decreases the emission by the surface and increases the emission by the atmosphere: the two terms compensate one another. On the other hand, a channel peaking around the tropopause generally mixes two parts of the temperature profile, one with a positive slope and one with a negative slope. Once again, an increase of CH_4 gives two signals compensating one another. The Jacobians have very similar shapes and all peak around 260 hPa. Hence, IASI only allows the retrieval of a mid-to-upper tropospheric integrated content of methane.

As seen on Figs. 1 and 2, infrared CH_4 sensitive channels are also essentially sensitive to temperature. Hence, the simultaneous use of IASI infrared measurements, sensitive to both temperature and CH_4 variations, and of AMSU microwave measurements, only sensitive to temperature, allows separating these two effects. AMSU channels 6 and 7 will be used in the retrieval procedure since their temperature weighting functions, shown in Fig. 2d, are the closest to those of the selected IASI channels, with no sensitivity to the surface.

3.2 A non-linear inference scheme

The weakness of the signal induced on IASI brightness temperature (BT) by CH_4 variations, associated with the complexity (in particular its non-Gaussianity) of the relationship between CH_4 concentration and observed BT, makes it difficult to solve this inverse problem. Therefore, a non-linear inference method, based on the Multilayer Perceptron (MLP) neural network (Rumelhart et al., 1986) with two hidden layers, has

been preferred to a more classical one. This method has already been used to derive tropospheric CO_2 integrated content from TOVS (Chédin et al., 2003, 2008), AIRS (Crevoisier et al., 2004) and IASI (Crevoisier et al., 2009). A detailed description of the method can be found in these references.

The chosen neural architecture is the following. The input layer is composed of: (1) the 9 IASI BT of the tropospheric channels given in Table 1, (2) 2 AMSU BT of channels 6 and 7, and (3) 2 differences between IASI and AMSU BT, to help constrain the convergence process. All together, there are 13 predictors. The output layer of the network is composed of: (1) the difference between the "true" value of CH_4 concentration (associated with inputs) and the "reference" one (1860 ppbv), and (2) 9 differences between the "true" IASI BT (associated with the true CH_4 concentration value) and the "reference" one (associated with the reference CH_4 concentration value), once again to constrain the solution. All together, there are 10 predictands.

The TIGR database (see Sect. 2.2) is used as the training set from which the networks learn the relationship existing between inputs and outputs. Network input BT correspond to randomly drawn values of CH_4 concentration in the range 1700–1900 ppbv and are computed from the reference value in TIGR using the CH_4 Jacobians. It is worth noting that no prior information is thus given to the networks in terms of seasonality, trend, or geographical patterns of methane.

Our past experience and several trials have led us to choose 70 neurons for the first hidden layer and 40 for the second one. Use is made of the Error Back-Propagation learning algorithm (Rumelhart et al., 1986), with stochastic steepest descent. At each step of the learning phase, the instrument noise is taken into account by adding to the BT of each channel a random Gaussian noise characterized by the equivalent noise temperature ($NE\Delta T$) computed at the BT of the channel, according to Eq. (1). A total of 7 MLPs have been trained, one for each of the first seven AMSU local zenithal angle, ranging from nadir to an upper limit of 40° to avoid the edges of the orbits.

As stated before, IASI channels are mostly sensitive to tropospheric variations of methane. The averaging kernels, which indicate which part of the atmosphere the

retrievals are representative of, are determined through radiative transfer simulations based on the TIGR atmospheric profiles not used in the training of the neural networks. A uniform perturbation of CH_4 mixing ratio is applied sequentially to each of the 40 layers of the atmospheric profiles. IASI and AMSU brightness temperatures are then computed for each of the perturbed atmospheric profiles and used as inputs of the neural network. The theoretical change F_i in ppmv/ppmv of the column mean apparent mixing ratio ($\hat{q}$) given a mixing ratio perturbation of Δq^{ref} at level i, is then given by

$$F_i = \frac{\hat{q}\left(\Delta q_i = \Delta q^{\text{ref}}\right) - \hat{q}\left(\Delta q_i = 0\right)}{\Delta q^{\text{ref}}} \quad (2)$$

The mean and standard deviation of the averaging kernel for the IASI CH_4 retrieval is plotted in Fig. 3. In the Tropics, the height of the tropopause is approximately 17 km. Thus, the non linear inference scheme described above gives access to a mid-to-upper tropospheric integrated content of CH_4 covering the range 100–500 hPa (roughly 5–15 km), with the highest sensitivity around 230 hPa.

3.3 Radiative bias removal

The MLPs are trained with simulated data. Therefore, before presenting observations to the networks, potential radiative systematic biases existing between simulations and observations must be removed. For each channel, the bias is obtained by averaging, over the first year of operation (July 2007–August 2008) and over the whole Tropics (20° S, 20° N), the differences between simulations, based on the forward model used and radiosonde measurements from the ECMWF ERA-40 database, and collocated (in time and space) satellite observations.

4 Results and discussion

Based on the non-linear inference scheme described in Sect. 3, 16 months, from July 2007 to October 2008, of coupled IASI and AMSU observations have been interpreted in terms of a tropospheric integrated content of CH_4 in the tropical belt (20° N, 20° S), over sea, at night, for clear-sky only. Cloud detection scheme is based on Crevoisier et al. (2009).

4.1 Potential perturbations of the retrievals

Through the careful selection described in Sect. 3.1, IASI channels used in the estimation process have a reduced sensitivity to water vapor. It is nonetheless required to verify that the neural networks have successfully been able to decorrelate CH_4 from water vapor. Similarly, the separation between temperature and CH_4 through the use of simultaneous infrared and microwave observations has to be validated. To perform this analysis, we use IASI Level 2 temperature and water vapor products (see Sect. 2.1), which have the advantage of being estimated directly from IASI: they thus describe precisely the state of the atmosphere at the locations we estimate CH_4. The coefficient of linearity R between our estimates of tropospheric CH_4 and either IASI Level 2 temperature at 200 hPa (maximum of IASI CH_4 averaging kernel plotted in Fig. 3) or water vapor contained in the troposphere (between 100 and 500 hPa) are 0.00 and 0.10, respectively. Both products are totally decorrelated; there is no remaining contamination of CH_4 retrievals from neither atmospheric temperature nor water vapor.

4.2 Seasonal cycles

Figure 4 shows the monthly zonal average of IASI CH_4 retrievals for 8 latitudinal bands of 5° each from 20° N to 20° S, over the Pacific Ocean. Since contrary to CO_2 and CO, no systematic aircraft measurement of methane is available in the Tropics, only measurements of methane made at the surface can be used to evaluate these results. Few

sites are available in this region. They provide some information on the expected seasonality and latitudinal variation of methane, which is a combination of various seasonal phenomena: sources (wetlands, termites, biomass burnings, anthropogenic), sinks (chemical destruction by OH), and atmospheric transport. Figure 5 shows the monthly evolution of CH_4 measured at 5 stations from the GLOBALVIEW-CH_4 (2008) network: MLO (19.53° N, 155.57° W, 3.4 km), KUM (19.52° N, 154.82° W, 3 m), GMI (13.43° N, 144.78° E, 2 m), CHR (1.70° N, 157.17° W, 3 m), and SMO (14.24° S, 170.57° W, 42 m), for the period July 2004–December 2007.

Both the IASI retrievals and the surface measurements show a strong North-to-South gradient. In the Northern Tropics, the seasonality retrieved from IASI is in agreement with in-situ observations: a strong seasonal cycle is observed, with a minimum in July–August and a maximum in November–February. However, the decrease of methane starts earlier on the retrieved IASI cycle (March) than at the surface (April to June, depending on the year). The amplitude of the IASI cycle, representative of the mid-to-upper troposphere, is about 40 ppbv, lower than the amplitude observed at the surface by about 20 ppbv. In the 5° N-EQ band, the global variation of IASI methane agrees well with what is observed at CHR (1.7° N). The early decrease in CH_4 from February to April retrieved by IASI is also sometimes observed at CHR, as in 2006. After almost a decade of constant globally-averaged atmospheric methane abundance (Dlugokencky et al., 2003), a renewed global growth of about 10 ppbv.year^{-1} is observed at all stations since the beginning of 2007 (Rigby et al., 2008). Such an increase is also retrieved by IASI as seen from comparing the months of July–September 2007 and the same months in 2008. A longer period is however required to confirm this tendency.

In the Southern Tropics, no clear seasonal cycle is retrieved from IASI. This is in agreement with the relatively weak seasonal cycle observed in-situ. A peak of 10 ppbv is observed by IASI in January–February 2008. These two months correspond to a rather high inter-annual variability observed at SMO for the period January to March. For instance, the seasonal cycles observed at SMO in the Southern Hemisphere and at the other sites in the Northern Tropics tend to be negatively correlated in 2005 (min-

imum of methane in boreal winter at SMO and maximum at the northern stations) but positively correlated in 2006–2007 (maximum of methane in January–February in both the Northern and Southern Tropics). This particular signal seems to be due to year-to-year fluctuations in interhemispheric transport during January–March, which tends to cancel the summer minimum, mainly due to photochemical destruction of methane (Dlugokencky et al., 1994), observed in the Southern Hemisphere at higher latitude (Prinn et al., 1992).

According to Figs. 4 and 5, the North-to-South latitudinal variation of methane retrieved from IASI is lower than the one observed at the surface. To evaluate this result, we use measurements of methane performed by aircraft in the troposphere at 11 km (thus close to the maximum of IASI averaging kernel plotted in Fig. 3), over the Pacific, between April and September 1993 (Matsueda and Inoue, 1996). The latitudinal variations of methane, averaged over the period April to September, as observed by IASI in 2008 and by the aircraft in 1993 are plotted in Fig. 6 (for comparison purposes, IASI values have been adjusted to the 1993 methane average). Tropospheric methane observed by IASI increases from the South to the North by about 30 ppbv. This is in excellent agreement with the aircraft measurements. From the five stations used above, the same latitudinal variation is observed at the surface, but with much larger amplitude (about 70 ppbv). As observed on both Figs. 4 and 6, methane is well-mixed in the Southern Tropics while a gradient persists with methane regularly increasing with latitude in the Northern Tropics.

4.3 Geographic distribution

Maps of seasonal mean CH_4 concentration are shown in Fig. 7 from September 2007 to August 2008, at a spatial resolution of 5°×5° (1°×1° moving average). This resolution was chosen to average enough individual retrievals to make robust statistics. After the removal of not-clear observations, the number of individual retrievals, per month and per 5°×5° gridbox, is about 400 in regions where clear-sky is prevailing but can be as low as 10 in more cloudy areas. To eliminate possible undetected clouds, boxes

having less than 40 individual retrievals are not considered (blank areas on Fig. 7). They mostly correspond to regions of deep convection with persistent cloudiness.

To compare this satellite product to MOZART-2 simulations, it is necessary to properly take into account the vertical weighting function F_i of the retrieval algorithm given by Eq. (2) in ppmv/ppmv. Since a given variation of the mixing ratio in two pressure layers with different thicknesses does not imply the same variation of molecules in each layer, translating F_i to the vertical discretization of MOZART-2 requires normalizing the function by the TIGR layer thickness ΔP_i on which F_i has been computed. This results in the molecular weighting function G_i

$$G_i = \frac{\sum_{j=1}^{N} \Delta P_j}{\Delta P_i} F_i \tag{3}$$

where N is equal to 40, the number of TIGR pressure layers. The 40 G_i values are independent of the layer thickness and they can be interpolated to any vertical layer distribution. Note that they are normalized so that the sum of the G_i, weighted by layer pressure thickness, is 1. The simulated integrated content of CH_4, denoted $q_{CH_4}^{MOZ}$, is finally given by

$$q_{CH_4}^{MOZ} = \frac{\sum_{i=1}^{M} H_i \Delta p_i q_i}{\sum_{i=1}^{M} H_i \Delta p_i} \tag{4}$$

where H_i is the vertical weithing function G_i interpolated on the M pressure layers Δp_i used by MOZART-2. Figure 8 shows the resulting integrated content of CH_4, averaged over 2000–2004, as simulated by MOZART-2, driven by NCEP winds and using the surface fluxes described in Sect. 2.3 as boundary conditions.

Overall, there is a good agreement between IASI and MOZART geographical patterns. However, the range of variation of IASI CH_4 is larger by about 20 ppbv, and the comparison of Figs. 7 and 8 shows a positive bias between retrieved and simulated methane. This result is in agreement with several studies based on satellite (Bergamaschi et al., 2007; Meirink et al., 2008) or aircraft measurements in the Tropics (Miller et

al., 2007), which have indicated significantly larger tropical emissions than previously reported. According to IASI, and in agreement with aircraft measurements performed at MLO, the magnitude of the simulated CH_4 is too low by about 20 ppbv. This might indicate too weak convection in the atmospheric model. Such limitation of atmospheric models has been reported in several studies (e.g., Stephens et al., 2007).

General patterns observed by IASI, and simulated by MOZART-2, include a year-long low CH_4 region over most of the Pacific ocean, plumes of elevated CH_4 between Africa and South America, year-long high values over Asia and the adjacent oceanic basins, and a latitudinal and temporal variation in agreement with in-situ observations. Also seen on the simulations, a plume of CH_4 can be observed originating from Central and Northern South America from August to September, where very large methane emissions have been retrieved by SCIAMACHY (Frankenberg et al., 2005). However, the signal observed by IASI, and simulated by MOZART-2, is much lower than observed by Frankenberg et al. (2005), in agreement with a revised version of SCIAMACHY results (Frankenberg et al., 2008).

Plumes of methane retrieved west of Africa show a latitudinal variation with the season. According to IASI, in boreal winter, methane is transported out of Africa towards the Atlantic Ocean mainly through the coast of Central Africa (10° N, 10° S), which might indicate large emissions of CH_4 from this region; in boreal summer, methane exits from West Africa (5° N, 15° N). This time-latitude variation is in agreement with the seasonality of methane emissions from African wetlands (Bergamaschi et al., 2007).

A particularly strong signal is the large plume of CH_4 retrieved south of the Asian continent from October to April, which agrees very well with model simulations. This large plume, which originates south of the Tibetan Plateau during the Asian summer monsoon, which is also the period of high emissions from rice paddies (Huang et al., 2004), seems to get first transported in the troposphere by deep convection and then tends to go South to reach Indonesia. Unfortunately, the persistent cloudiness over the Asian continent from July to September precludes IASI from seeing the beginning of the plume. In boreal winter, emissions become stronger over Indonesia. Comparisons

between MOZART-2 simulations and IASI retrievals show that IASI observes a much larger dispersion of the plume over the nearby oceanic basins. This might explain part of the peak of CH_4 seen on the seasonal variation in the Southern Tropics plotted in Fig. 5. The high values of CH_4 retrieved by IASI in boreal winter may also be explained by transport of air with elevated CH_4 from the Northern Hemisphere where methane emissions are at their maximum.

In the absence of observed global maps of tropospheric CH_4, a first way of quantifying the dispersion of the retrievals is to determine the standard deviation of each monthly 5°×5° box item sample. A small dispersion of 19 ppbv is observed (less than 1% of the mean CH_4 mixing ratio), which partly comes from the errors due to the method and to the instrument, and partly from the natural variability of methane within each box over one month. The smallest values of the standard deviation (∼17 ppbv) correspond to the months of July–September when the natural variability (and the concentration, in particular in the Northern Tropics) is at its minimum, and the maximum values (∼21 ppbv) correspond to the months of January–March when the natural variability (and the concentration, in particular in the Northern Tropics) is at its maximum. Following Chédin et al. (2003), these standard deviations may tentatively be seen as resulting from the combination of the standard deviation of the method (σ_M) itself and of the standard deviation of the natural variability (σ_V) of CH_4 (5°×5°, one month). Doing so, σ_M comes to about 16 ppbv (∼0.9%) and σ_V comes to 3 ppbv in July–September and to 13 ppbv in January–March. Such numbers look reasonable. However, this result is more an appreciation of the internal consistency of the method than an estimation of its accuracy.

Associated with the comparison to in situ measurements and atmospheric transport model simulations, these values bring some confidence in the overall description of the features of the CH_4 field variability. More detailed analysis of the results and comparisons with other satellite data will be the subject of a follow-on paper.

5 Conclusions

With its high spectral resolution and low radiometric noise, IASI provides new capabilities to monitor methane in the troposphere. Nine channels, located in band ν_4 of methane near 7.7 μm, present high sensitivities to methane, reduced sensitivities to water vapor, and no sensitivity to nitrous oxide and surface characteristics. They are mostly sensitive to methane variations in the mid-to-upper troposphere, thus leading to the retrieval of a mid-to-upper tropospheric integrated content representative of the 5–15 km range in the Tropics through the use of a non-linear inference scheme based on neural networks. The retrievals, performed for clear-sky only, agree well with in-situ measurements in terms of seasonality, annual increase and latitudinal variation. Comparisons with simulations from an atmospheric transport and chemistry model give confidence in the ability of IASI to detect the geographical distribution of tropospheric methane.

It is worth noting that the IASI CH_4 retrieval scheme does not use any a priori information on the trend, the seasonality, nor the geographical distribution of methane. Likewise, the IASI CH_4 retrievals are fully independent from any a priori knowledge of the state of the atmosphere and do not rely on any Level 2 data. It has been demonstrated that the method has fully decorrelated methane from water vapor and temperature variations. This has been achieved by using observations performed simultaneously by IASI, sensitive to both temperature and methane, and AMSU, only sensitive to temperature. The performance of the retrieval is thus linked to both IASI and AMSU instruments. The accuracy of the retrieval has been found to be about 16 ppbv (∼0.9%), for a 5°×5° spatial resolution on a monthly time scale. However, validation in the upper troposphere is challenging due to lack of direct measurements.

As illustrated by the detection of a plume of elevated methane in the late summer over the Pacific, which can be attributed to Asian emissions uplifted to the troposphere, IASI retrievals present a means to detect atmospheric transport pathways and to improve our knowledge on the mechanisms that transport methane emissions from the

surface to the upper atmosphere. While not sensitive to surface methane, IASI observations might thus prove useful for constraining atmospheric transport in a so-called surface flux inversion. The retrievals being only performed in clear-sky conditions, it is however needed to take this into account while performing any estimate of sources and sinks. With the launch of two other successive IASI-like instruments, scheduled for 2011 and 2015, more than 20 years of methane will be available for climate studies.

Acknowledgements. This work has been supported in part by the European Community under the contract FP6-516099 ("GEMS"). We particularly wish to thank C. Boone and the Ether team for their help in getting IASI data. We gratefully acknowledge G. Dufour for fruitful discussions. IASI has been developed and built under the responsibility of the Centre National d'Etudes Spatiales (CNES, France). It is flown onboard the Metop satellites as part of the EUMETSAT Polar System. The IASI L1 data are received through the EUMETCast near real time data distribution service.

The publication of this article is financed by CNRS-INSU.

References

Bergamaschi, P., Frankenberg, C., Meirink, J. F., Krol, M., Dentener, F., Wagner, T., Platt, U., Kaplan, J. O., Körner, S., Heimann, M., Dlugokencky,E. J., and Goede, A.: Satellite chartography of atmospheric methane from SCIAMACHY on board ENVISAT: 2. Evaluation based on inverse model simulations, J. Geophys. Res., 112, D02304, doi:10.1029/2006JD007268, 2007. 6869, 6870

Bousquet, P., Ciais, P., Miller, J. B., Dlugokencky, E. J., Hauglustaine, D. A., Prigent, C., Van

der Werf, G. R., Peylin, P., Brunke, E.-G., Carouge, C., Langenfelds, R. L., Lathi/Are, J., Papa, F., Ramonet, M., Schmidt, M., Steele, L. P., Tyler, S. C., and White, J.: Contribution of anthropogenic and natural sources to atmospheric methane variability, Nature, 443(7110), 439–443, 2006. 6857

Buchwitz, M., de Beek, R., Noël, S., Burrows, J. P., Bovensmann, H., Schneising, O., Khlystova, I., Bruns, M., Bremer, H., Bergamaschi, P., Körner, S., and Heimann, M.: Atmospheric carbon gases retrieved from SCIAMACHY by WFM-DOAS: version 0.5 CO and CH_4 and impact of calibration improvements on CO_2 retrieval, Atmos. Chem. Phys., 6, 2727–2751, 2006, http://www.atmos-chem-phys.net/6/2727/2006/. 6858

Chédin, A., Scott, N. A., Wahiche, C., and Moulinier, P.: The improved initialisation inversion method: A high resolution physical method for temperature retrievals from satellites of the TIROS-N series, J. Clim. Appl. Meteorol., 24, 128–143, 1985. 6860

Chédin, A., Serrar, S., Scott, N. A., Crevoisier, C., and Armante, R.: First global measurement of mid-tropospheric CO_2 from NOAA polar satellites: Tropical zone, J. Geophys. Res., 108(D18), 4581, doi:10.1029/2003JD003439, 2003. 6864, 6871

Chédin A., Scott, N. A., Armante, R., Pierangelo, C., Crevoisier, C., Fossé, O., and Ciais, P.: A quantitative link between CO_2 emissions from tropical vegetation fires and the daily tropospheric excess (DTE) of CO_2 seen by NOAA-10 (1987–1991), J. Geophys. Res., 113, D05302, doi:10.1029/2007JD008576, 2008. 6864

Chen, Y.-H. and Prinn, R. G.: Estimation of atmospheric methane emissions between 1996 and 2001 using a three-dimensional global chemical transport model, J. Geophys. Res., 111, D10306, doi:10.1029/2005JD006058, 2006. 6857

Chevallier, F., Chéruy, F., Scott, N. A., and Chédin, A.: A neural network approach for a fast and accurate computation of a longwave radiative budget, J. Appl. Meteorol., 37, 1385–1397, 1998. 6860

Cicerone R. J. and Oremland, R. S.: Biogeochemical aspects of atmospheric methane, Global Biogeochem. Cy., 2, 299–237, 1988. 6857

Clerbaux, C., Hadji-Lazaro, J., Turquety, S., Mégie, G., and Coheur, P.-F.: Trace gas measurements from infrared satellite for chemistry and climate applications, Atmos. Chem. Phys., 3, 1495–1508, 2003, http://www.atmos-chem-phys.net/3/1495/2003/. 6858

Crevoisier, C., Chédin, A., and Scott, N. A.: AIRS channel selection for CO_2 and other trace-gas retrievals, Q. J. Roy. Meteorol. Soc., 129, 2719–2740, 2003. 6862, 6863

Crevoisier, C., Heilliette, S., Chédin, A., Serrar, S., Armante, R., and Scott, N. A.: Midtropospheric CO_2 concentration retrieval from AIRS observations in the tropics, Geophys. Res. Lett., 31, L17106, doi:10.1029/2004GL020141, 2004. 6864

Crevoisier, C., Chédin, A., Matsueda, H., Machida, T., Armante, R., and Scott, N. A.: First year of upper tropospheric integrated content of CO_2 from IASI hyperspectral infrared observations, Atmos. Chem. Phys., submitted, 2009.

Dlugokencky, E. J., Steele, L. P., Lang, P. M., and Masarie, K. A.: The growth rate and distribution of atmospheric methane, J. Geophys. Res., 99(D8), 17021–17043, 1994. 6868

Dlugokencky, E. J., Houweling, S., Bruhwiler, L., Masarie, K. A., Lang, P. M., Miller, J. B., and Tans, P. P.: Atmospheric methane levels off: Temporary pause or a new steady-state?, Geophys. Res. Lett., 30(19), 1992, doi:10.1029/2003GL018126, 2003. 6867

EUMETSAT: EPS Ground segment, IASI Level2 Product Generation Specification, EPS.SYS.SPE.990013 EUMETSAT Technical Note, online available at: http://www.eumetsat.int/, last access: 2009, 2004. 6860

Fiore, A. M., Horowitz, L. W., Dlugokencky, E. J., and West, J.: Impact of Meteorology and Emissions on Methane Trends, 1990–2004, Geophys. Res. Lett., 33, L12809, doi:10.1029/2006GL026199, 2006. 6861

Frankenberg, C., Meirink, J. F., van Weele, M., Platt, U., and Wagner, T.: Assessing methane emissions from global space-borne observations, Science, 308, 1010–1014, doi:10.1126/science.1106644, 2005. 6858, 6870

Frankenberg, C., Meirink, J. F., Bergamaschi, P., Goede, A. P. H., Heimann, M., Körner, S., Platt, U., VanWeele, M., and Wagner, T.: Satellite chartography of atmospheric methane from SCIAMACHYon board ENVISAT: Analysis of the years 2003 and 2004, J. Geophys. Res., 111, D07303, doi:10.1029/2005JD006235, 2006. 6858

Frankenberg, C., Bergamaschi, P., Butz, A., Houweling, S., Meirink, J. F., Notholt, L., Petersen, A. K., Schrijver, H., Warneke, T., and Aben, I.: Tropical methane emissions: A revised view from SCIAMACHY onboard ENVISAT, Geophys. Res. Lett., 35, L15811, doi:10.1029/2008GL034300, 2008. 6858, 6870

Fung, I., John, J., Lerner, J., Matthews, E., Prather, M., Steele, L. P., and Fraser, P. J.: Three-Dimensional Model Synthesis of the Global Methane Cycle, J. Geophys. Res., 96(D7), 13033–13065, 1991.

GLOBALVIEW-CH_4: Cooperative Atmospheric Data Integration Project – Methane, CD-ROM, NOAA ESRL, Boulder, Colorado, online available on Internet via anonymous FTP to

ftp.cmdl.noaa.gov, Path: ccg/ch4/GLOBALVIEW, 2008. 6867

Harris, J. M., Tans, P. P., Dlugokencky, E. J., Masarie, K. A., Lang, P. M., Whittlestone, S., and Steele, L. P.: Variations in Atmospheric Methane at Mauna Loa Observatory Related to Long-Range Transport, J. Geophys. Res., 97(D5), 6003–6010, 1992.

Horowitz, L. W., Walters, S., Mauzerall, D. L., Emmons, L. K., Rasch, P. J., Granier, C., Tie, X., Lamarque, J.-F., Schultz, M. G., Orlando, G. S. T. J. J., and Brasseur, G. P. : A global simulation of tropospheric ozone and related tracers: Description and evaluation of MOZART, version 2, J. Geophys. Res., 108(D24), 4784, doi:10.1029/2002JD002853, 2003. 6861

Houweling, S., Kaminski, T., Dentener, F., Lelieveld, J., and Heimann, M.: Inverse modeling of methane sources and sinks using the adjoint of a global transport model, J. Geophys. Res., 104 (D21), 26137–26160, 1999. 6857

Huang, Y., Zhang, W., Zheng, X. H., Li, J., and Yu, Y. Q.: Modeling methane emission from rice paddies with various agricultural practices, J. Geophys. Res.-Atmos., 109, D08113, doi:10.1029/2003JD004401, 2004. 6857, 6870

IPCC: Climate Change 2007, in: The Physical Science Basis. Contribution of Working Group I to the Fourth Assessment Report of the Intergovernmental Panel on Climate Change, edited by: Solomon, S., Qin, D., Manning, M., Chen, Z., Marquis, M., Averyt, K. B., Tignor, M., and Miller, H. L., Cambridge University Press, Cambridge, UK and New York, NY, USA, 996 pp., 2007. 6857

Jacquinet-Husson, N., Scott, N. A., Chédin, A., Crépeau, L., Armante, R., Capelle, V., and 47 co-authors: The GEISA spectroscopic database: Current and future archive for Earth and planetary atmosphere studies., J. Quant. Spectrosc. Ra., 109, 1043–1059, 2008. 6860

Logan, J. A., Prather, M. J., Wofsy, S. C., and McElroy, M. B.: Tropospheric chemistry: a global perspective, J. Geophys. Res., 86, 7210–7254, 1981. 6857

Matsueda, H. and Inoue, H. Y.: Measurements of atmospheric CO_2 and CH_4 using a commercial airliner from 1993 to 1994, Atmos. Environ., 30, 1647–1655, 1996. 6868

Matthews, E. and Fung, I.: Methane emissions from natural wetlands: Global distribution, area, and ecology of sources, Global Biogeochem. Cy., 1, 61–86, 1987. 6861

Meirink, J. F., Bergamaschi, P., and Krol, M. C.: Four-dimensional variational data assimilation for inverse modelling of atmospheric methane emissions: method and comparison with synthesis inversion, Atmos. Chem. Phys., 8, 6341–6353, 2008, http://www.atmos-chem-phys.net/8/6341/2008/. 6869

Mikaloff-Fletcher, S. E., Tans, P. P., Bruhwiler, L. M., Miller, J. B., and Heimann, M.: CH_4

sources estimated from atmospheric observations of CH_4 and its $^{13}C/^{12}C$ isotopic ratios: 1. Inverse modeling of source processes, Global Biogeochem. Cy., 18, GB4004, doi:10.1029/2004GB002223, 2004a. 6857

Mikaloff-Fletcher, S. E., Tans, P. P., Bruhwiler, L. M., Miller, J. B., and Heimann, M.: CH_4 sources estimated from atmospheric observations of CH_4 and its $^{13}C/^{12}C$ isotopic ratios: 2. Inverse modeling of CH_4 fluxes from geographical regions, Global Biogeochem. Cy., 18, GB4004, doi:10.1029/2004GB002224, 2004b. 6857

Miller, J., Gatti, L., d'Amelio, M., Crotwell, A., Dlugokencky, E., Bakwin, P., Artaxo, P., and Tans, P. P.: Airborne measurements indicate large methane emissions from the eastern Amazon basin, Geophys. Res. Lett., 34, L10809, doi:10.1029/2006GL029213, 2007. 6869

Olivier, J. G. J. and Berdowski, J. J. M.: Global emissions sources and sinks, in: The Climate System, edited by: Berdowski, J., Guicherit, R., and Heij, B. J., et al., A. A. Balkema, Brookfield, VT, UK, 33–78, 2001. 6861

Olivier, J. G. J., Aardenne van, J. A., Dentener, F. J., Pagliari, V., Ganzeveld, L. N., and Peters, J. A. H. W.: Recent trends in global greenhouse gas emissions: Regional trends and spatial distribution of key sources, in: Non-CO_2 Greenhouse Gases (NCGG-4), edited by: van Amstel, A., Millpress, Rotterdam, The Netherlands, 325–330, 2005. 6861

Park, J. H., Russell, J. M., Gordley, L. L., Drayson, S. R., Benner, D. C., McInerney, J. M., Gunson, M. R., Toon, G. C., Sen, B., Blavier, J.-F., Webster, C. R., Zipf, E. C., Erdman, P., Schmidt, U., and Schiller, C.: Validation of Halogen Occultation Experiment CH_4 measurements from the UARS, J. Geophys. Res., 101(D6), 10183–10204, 1996. 6858

Prentice, I. C., Farquhar, G. D., Fasham, M. J. R., Goulden, M. L., Heimann, M., Jaramillo, V. J., Keshgi, H. S., LeQuéré, C., Scholes, R. J., and Wallace, D. W. R.: IPCC, WGI Third Assessment Report, Cambridge University Press, Cambridge, UK, 2001. 6857

Prinn, R., Cunnold, D., Simmonds, P., Alyea, F., Boldi, R., Crawford, A., Fraser, P., Gutzler, D., Hartley, D., Rosen, R., and Rasmussen, R.: Global Average Concentration and Trend for Hydroxyl Radicals Deduced From ALE/GAGE Trichloroethane (Methyl Chloroform) Data for 1978–1990, J. Geophys. Res., 97(D2), 2445–2461, 1992. 6868

Randel, W. J., Wu, F., Russell III, J. M., Roche, A., and Waters, J. W.: Seasonal cycles and QBO variations in stratospheric CH_4 and H_2O observed in UARS HALOE data, J. Atmos. Sci., 55, 163–185, 1998. 6858

Rayner, P. J. and O'Brien, D. M.: The utility of remotely sensed CO_2 concentration data in surface source inversions, Geophys. Res. Lett., 28(1), 175–178, 2001. 6857

Rigby, M., Prinn, R. G., Fraser, P. J., Simmonds, P. G., Langenfelds, R. L., Huang, J., Cunnold, D. M., Steele, L. P., Krummel, P. B., Weiss, R. F., O'Doherty, S., Salameh, P. K., Wang, H. J., Harth, C. M., Mühle, J., and Porter, L. W.: Renewed growth of atmospheric methane, Geophys. Res. Lett., 35, L22805, doi:10.1029/2008GL036037, 2008. 6867

Rumelhart, D. E., Hinton, G. E., and Williams, R. J.: Learning internal representations by error propagation, in: Parallel Distributed Processing: Explorations in the Macrostructure of Cognition, vol. 1, edited by: Rumelhart, D. E. and McClelland, J. L., MIT Press, Cambridge, Mass, UK, 318–362, 1986. 6863, 6864

Schoeberl, M. R., Luo, M., and Rosenfield, J. E.: An analysis of the Antarctic Halogen Occultation Experiment trace gas observations, J. Geophys. Res., 100, 5159–5172, 1995. 6858

Scott, N. A. and Chédin, A.: A fast line-by-line method for atmospheric absorption computations: The Automatized Atmospheric Absorption Atlas, J. Appl. Meteorol., 20, 556–564, 1981. 6860

Spivakovsky, C. M., Logan, J. A., Montzka, S. A., Balkanski, Y. J., Foreman-Fowler, M., Jones, D. B. A., Horowitz, L. W., Fusco, A. C., Brenninkmeijer, C. A. M., Prather, M. J., Wofsy, S. C., and McElroy, M. B.: Three-dimensional climatological distribution of tropospheric OH: Update and evaluation, J. Geophys. Res., 105(D7), 8931–8980, doi:10.1029/1999JD901006, 2000. 6857

Stephens, B. B., Gurney, K. R., Tans, P. P., Sweeney, C., Peters, W., Bruhwiler, L., Ciais, P., Ramonet, M., Bousquet, P., Nakazawa, T., Aoki, S., Machida, T., Inoue, G., Vinnichenko, N., Lloyd, J., Jordan, A., Heimann, M., Shibistova, O., Langenfelds, R. L., Steele, L. P., Francey, R. J., and Denning, A. S.: Weak northern and strong tropical land carbon uptake from vertical profiles of atmospheric CO_2, Science, 316, 1732–1735, doi:10.1126/science.1137004, 2007. 6870

Wang, J. S., Logan, J. A., McElroy, M. B., Duncan, B. N., Megretskaia, I. A., and Yantosca, R. M.: A 3-D model analysis of the slowdown and interannual variability in the methane growth rate from 1988 to 1997, Global Biogeochem. Cy., 18, GB3011, doi:10.1029/2003GB002180, 2004. 6861

Xiong, X., Barnet, C. D., Maddy, E. , Sweeney, C. , Liu, X. , Zhou, L., and Goldberg, M.: Characterization and Validation of Methane Products from the Atmospheric Infrared Sounder (AIRS), J. Geophys. Res., 113, G00A01, doi:10.1029/2007JG000500, 2008. 6858

Table 1. List of IASI channels selected to retrieve methane. Columns 3 to 8 indicate the sensitivity (in K) of each channel to the variation of CH_4 (10%), H_2O (20%), N_2O (2%), atmospheric temperature (1 K), surface temperature (1 K) and surface emissivity (0.01). Column 10 gives the pressure P_{max} of the maximum of the CH_4 Jacobians.

Channel	ω (cm^{-1})	CH_4 (K)	H_2O (K)	N_2O (K)	T (K)	T_{surf} (K)	ϵ_{surf} (K)	Noise (K)	P_{max} (hPa)
2628	1301.75	1.07	0.13	0.09	0.92	0.01	0.03	0.20	292
2634	1303.25	1.06	0.11	0.08	0.94	0.01	0.02	0.21	292
2635	1303.50	1.13	0.06	0.05	0.97	0.00	0.00	0.24	262
2636	1303.75	1.11	0.07	0.06	0.98	0.00	0.00	0.23	262
2637	1304.00	1.17	0.12	0.07	0.97	0.01	0.02	0.20	292
2638	1304.25	1.27	0.11	0.05	0.96	0.00	0.01	0.21	262
2639	1304.50	1.18	0.07	0.04	0.96	0.00	0.01	0.24	262
2640	1304.75	1.00	0.05	0.05	0.97	0.00	0.00	0.27	235
2641	1305.00	1.08	0.08	0.04	0.95	0.00	0.00	0.25	235

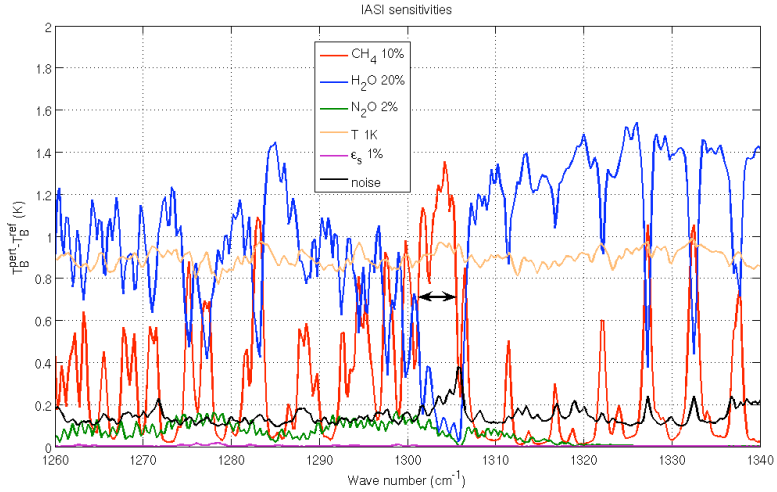

Fig. 1. Sensitivities of IASI channels located in the 7.7 μm band to variations of methane (10%), water vapor (20%), nitrous oxide (2%), atmospheric temperature (1 K), surface emissivity (0.01), and instrument noise computed at the brightness temperature. Average over the 4425 TIGR tropical atmospheric situations. Arrows denote the spectral range where channels selected to retrieve methane are located.

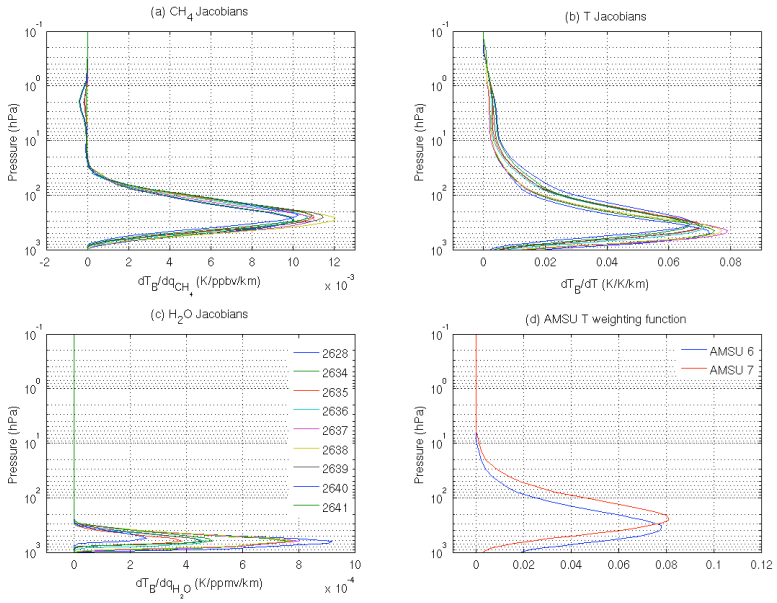

Fig. 2. CH_4 **(a)**, temperature **(b)** and H_2O **(c)** Jacobians of the 9 IASI channels selected to estimate methane, and **(d)** temperature weighting functions of AMSU channels 6 and 7 (average over the TIGR tropical atmospheric situations).

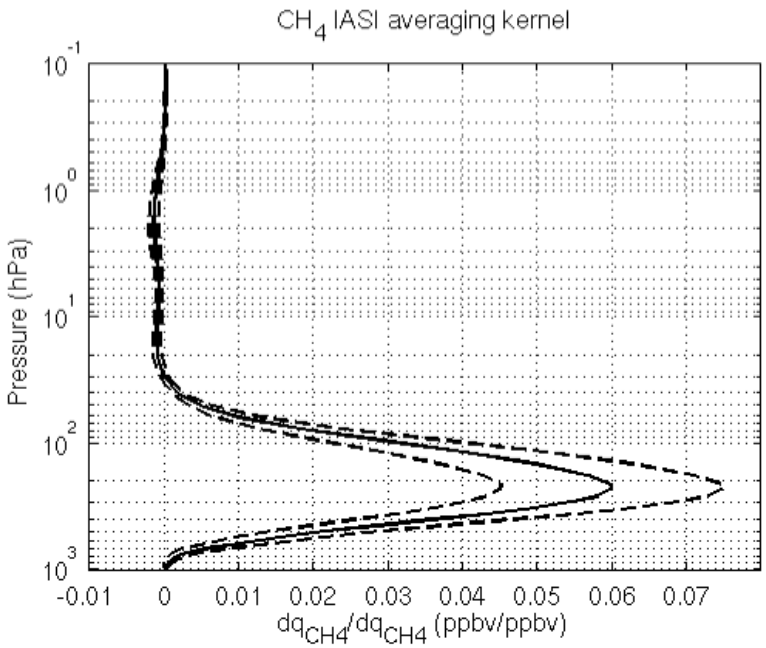

Fig. 3. Averaging kernel of CH_4 IASI retrieval. Mean (full line) plus or minus standard deviation (dashed lines) over the TIGR tropical atmospheric situations.

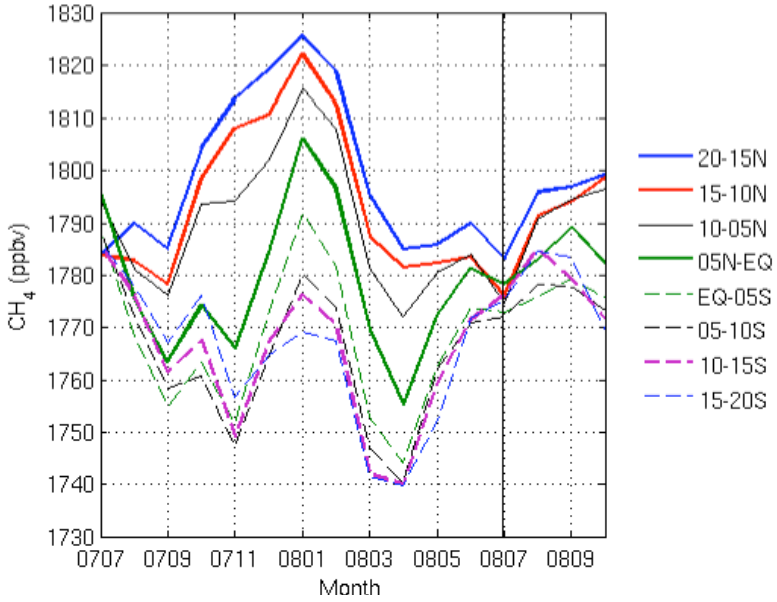

Fig. 4. Seasonal cycle of methane as retrieved in the mid-to-upper troposphere from IASI over the Pacific Ocean in 8 latitudinal bands of 5° each from July 2007 to October 2008.

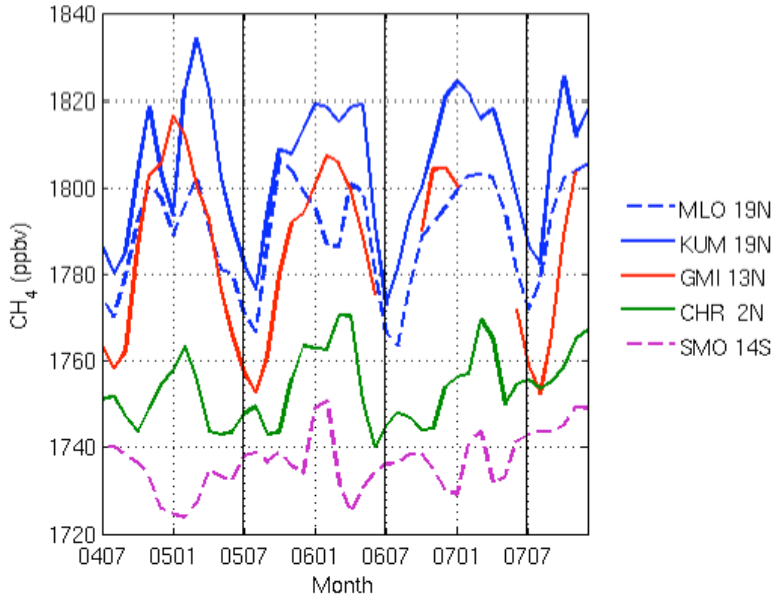

Fig. 5. Seasonal cycle of methane measured at the surface at 5 sites from July 2004 to December 2007.

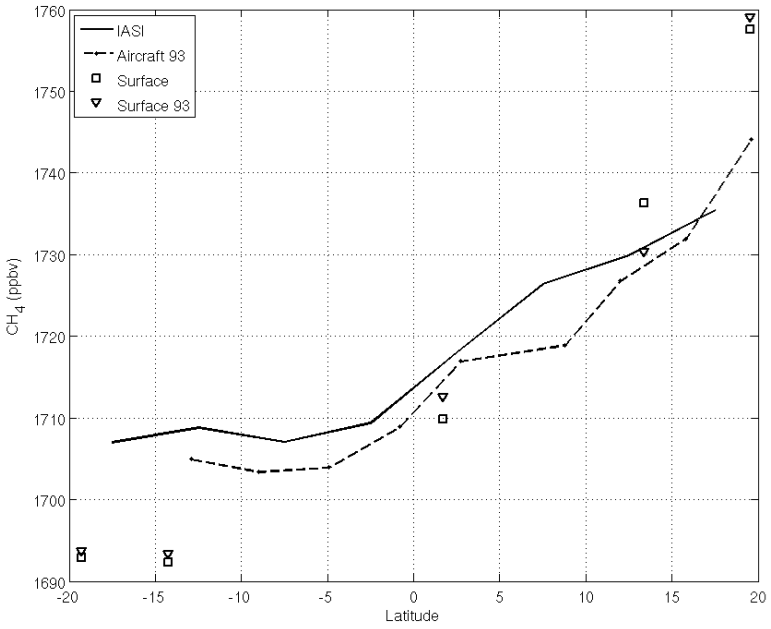

Fig. 6. Latitudinal variation of methane as retrieved in the mid troposphere from IASI (full line), as observed at 11 km by aircraft in 1993 (dashed line with circles), as observed at the surface in 2003–2006 (squares) and as observed at the surface in 1993 (triangles). For the sake of comparison, all curves have been adjusted to match the aircraft 1993 mean.

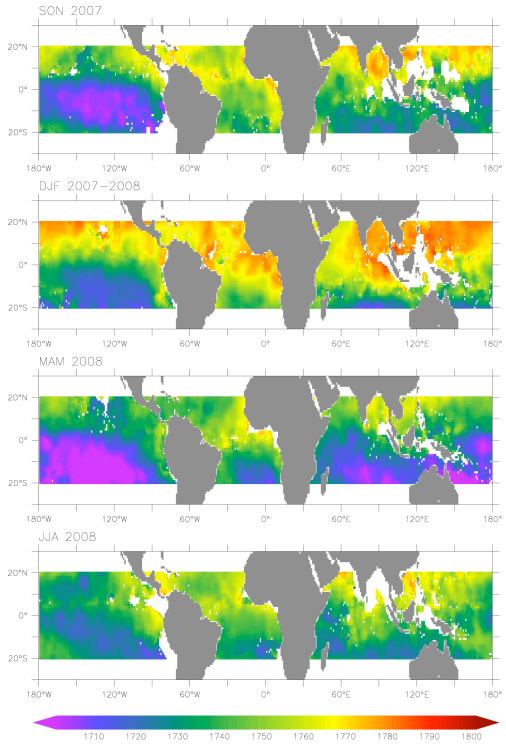

Fig. 7. Seasonal mid-to-upper tropospheric integrated content of methane (ppbv) as retrieved from IASI observations, from September 2007 to August 2008, at a resolution of 5°×5°.

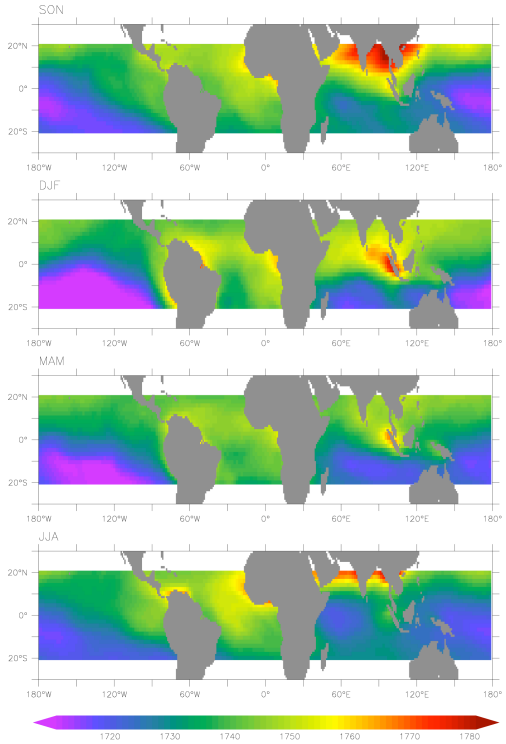

Fig. 8. Seasonal mid-to-upper tropospheric integrated content of methane (ppbv) as simulated by MOZART-2 and averaged over 2000–2004.